arXiv:1212.0592v1 [q-bio.NC] 4 Dec 2012

Using the scalp electric field to improve the recognition of brain processes

C. G. Carvalhaes* M. Perreau-Guimarães
P. Suppes
Center for the Study of Language and Information,
Stanford University, Stanford, CA 94305

J. Acacio de Barros
Liberal Studies, San Francisco State University,
1600 Holloway Ave, San Francisco, CA 94312

Abstract

This paper discusses the use of the scalp electric field to decode EEG-recorded brain processes. Instead of using bipolar measurements, the scalp electric field is described as a 3-vector field whose orthogonal components are obtained from the data through spline differentiation. The method was tested in the context of brainwave recognition with experiments involving brain representation of spoken phonemes, visual images, and mental images. The practical effect of improvements in recognition rates was assessed by estimating effect sizes and confidence intervals, the results suggesting a good prospect for other applications.

Introduction

Performing the surface Laplacian differentiation of scalp potentials has proved to be an efficient method to circumvent reference issues which may strongly influence coherence estimations of EEG signals (Hjorth, 1975; Perrin et al, 1989). Additionally, many studies suggested that dura-surface potential is more accurately represented using surface-Laplacian topography rather than conventional topography (Nunez and Pil-

---

*Email: claudioc@stanford.edu

green, 1991; Nunez et al, 1991; Nunez and Westdorp, 1994; Nunez et al, 1994; Srinivasan et al, 1996; Nunez and Srinivasan, 2006). This has motivated a number of experimental studies of both clinical and theoretical interest, such as those of Babiloni et al (1999, 2000, 2001, 2002); Chen et al (2005); Kayser and Tenke (2006a,b); Bai et al (2008); Besio et al (2009). Yet, despite the its broad success, we show in this paper that the surface-Laplacian differentiation gives an incomplete description of the physical process underlying EEG, in the sense that it corresponds to an approximation for the normal component of the *scalp electric field*. But in addition to the field's normal component, tangential components are potentially a valuable resource to supplement and enhance information not encoded in the surface-Laplacian differentiation. Based on this consideration, the scalp electric field is thereby regarded as the central quantity for overall assessment of the data content. Therefore, the estimation of the scalp electric field from empirical data is the principal subject of our current work.

At first glance, this seems not to be a new topic. Bipolar records over closely-spaced scalp sites have long been used to circumvent reference channel effects, and they are closely related to the value of the electric field along the scalp surface. This measure, however, leaves out the field's normal component that arises when resistive electrodes are attached to the scalp in order to acquire the signal. Our approach takes this component into account and fully reconstructs the scalp electric field as a 3-vector field at measuring sites. More importantly, our results consistently emphasize the significance of this full estimation to achieve optimal results.

We used splines to perform efficiently spatial differentiations to obtain the field components. As an application, we considered three experiments of brain-wave representation for which the effectiveness of the scalp electric field to improve recognition rates was statistically evaluated. These experiments involved brain processing of (*i*) spoken phonemes in consonant-vowel format; (*ii*) two-dimensional images of geometric shapes (circle, square, and triangle) filled in with different colors (red, green, and blue); and (*iii*) mental images in response to hear a "go" sound or view a "stop" sign on a computer screen. We used effect sizes with 95% confidence intervals to estimate the practical significance of improvements, yielding an optimistic prospect for further developments and applications of the proposed technique.

Methods

Experimental Procedures

We refer to the three experiments used in our study as Exp. I, Exp. II, and Exp. III. Briefly, Exp. I consisted of auditory presentations of 32 consonant-vowel syllables; Exp. II focused on the brain representation of 9 images formed from pairwise combinations of three shapes (circle, square, and triangle) and three colors (red, green, and blue); and Exp. III was a two-class imaginary task performed right after a stimulus presentation. These experiments were conducted on-site in our Laboratory motivated by different scientific purposes. The subjects who voluntarily took part in each experiment were all healthy adults who reported normal hearing, normal or correct-to-normal vision, and normal color vision. They were labeled as S1, S2, S3, $\cdots$, but participant S1 of Exp. I was not necessarily the same as participant S1 of Exp. II, and so on.

Exp. I: 32 consonant-vowel syllables

This experiment emerged from Rui Wang's doctoral work (Wang, 2011) and appeared recently in Wang et al (2012). The focus was on the identification of brain patterns induced by auditory syllable stimuli. EEG data were recorded from 4 participants (S1-S4), 1 male, who were engaged in the discrimination of 32 English syllables formed from pairwise combinations of the 8 consonants /p/, /t/, /b/, /g/, /f/, /s/, /v/, /z/, and 4 vowels /i/ (as in m**ee**t), /æ/ (c**a**t), /u/ (s**oo**n), and /a/ (sp**a**). These vowels were selected to facilitate recognition, as they are maximally separated in the American-English vowel space. The sounds of the syllables were uttered by a male native speaker of English, with 7 recordings being made for each syllable to create a diversity of speech signal. Participants were instructed to carefully listen to the spoken words and try to comprehend them, but no response was required. The stimuli were randomly presented via a computer speaker in sessions of 1000-ms trials. Each session lasted 15 minutes and consisted of 28 repetitions of each syllable, amounting to 896 trials per session. A total of 7,168 trials (8 sessions) were collected for participant S1; 3,584 (4 sessions) for S2; 6,272 (7 sessions) for S3; and 4,480 (5 sessions) for S4. There was a short break after each block of 56 trials, and the participant could control the length of the break by pressing the spacebar.

Exp. II: 9 shape-color images

This not-yet-published experiment, performed by researchers at the Suppes Brain Lab (P. Suppes, M. P. Guimarães, and ???), tested the recognition of brain-wave representations of nine two-dimensional images, formed by pairwise combining three geometric shapes (*circle*, *square*, *and triangle*) and three colors (*red*, *green*, and *blue*). The researchers presented randomly these images to seven participants (S1-S7), three female, on a 17-inch computer screen against a dark background. The area of each shape was approximately the same, and the physical luminosity was adjusted for each object and color to appear the same at one meter from the screen. No attempt was made to adjust images to each participant, such that the subjective perception of luminosity was the same for all colors and each participant. Each presentation lasted 300 ms with an inter-stimulus interval of 1000 ms. A white fix point ('+') lasting 700 ms was shown at the center of a blank screen, immediately after the presentation. Participants were instructed to remain relaxed and motionless, and to keep their eyes fixed at the center of the screen during presentations. In total 2,700 trials were performed per participant, with stimuli randomly appearing on the screen with equal probability. The presentations were divided in blocks of 20 trials and the participant could control the duration of the breaks via the spacebar. Halfway through the experiment a modified break message was displayed informing the participant that the experiment had passed its half point.

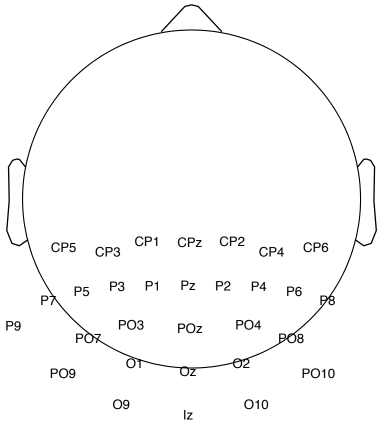

Figure 1: Electrode montage used in Experiment II.

Exp. III: 2-class imagery task

The third experiment was previously described in detail in Carvalhaes et al (2009); Carvalhaes and Suppes (2011). Eleven participants (S1-S11) were randomly presented on every other trial either a visual “stop” sign, flashed on a computer screen, or the sound of the English word “go”, uttered by a male native speaker of English. Each stimulus presentation lasted 300 ms, and was followed by a period of 700 ms of blank screen. Immediately after this period a fixation point (‘+’) was showed at the center of the screen for 300 ms. For one group (S1-S7) the participants were instructed to form a vivid mental image of the stimulus previously presented, for another group (S8-S11) they were asked to form a mental image of the alternative stimulus, i.e., if the last stimulus was the “stop” sign, then they should imagine the “go” sound, and vice versa. Participant’s imagining was followed by another 700 ms of blank screen, after which the trial ended. A single session of 600 trials was recorded for each participant. The session was divided into thirty 20-trial blocks, with regular breaks controlled by the participant via spacebar. Each trial lasted 2,000 ms, but only the last 1,000 ms of each trial corresponding to the imagination task was used for our analysis.

Data collection and preprocessing

The apparatus used to record EEG signals changed from an experiment to another. Exp. I was carried out using EGI’s Geodesic EEG system with 128 monopolar channels referenced to the vertex electrode (Cz). In Exp. II signals were recorded using a 32-channel NeuroScan system with linked earlobe reference. Due to the low number of channels available on this device – and in view of the need for a reasonable density of electrodes to accurately estimate the electric field in the region of interest (V1) – the measurement electrodes were all placed in the back part of the head, as depicted in Figure 1. Exp. III used a 64-channel Neuroscan system, following the 5% system of Oostenveld and Praamstra (2001), but not including electrodes Nz, AF1, AF2, AF5, AF6, T9, T10, P9, P5, P6, P9, P10, PO, or I. All signals were recorded in an audio isolation, darkened room. After amplification, the signals were passed through a band-pass filter in the range 0.1-300 Hz plus a 60 Hz notch filter. The conversion into digital form was performed at a sampling rate of 1 kHz.

To reduce features, we then carried out offline decimation at 16:1 ratio, thus setting the Nyquist frequency at 31.25 Hz. Additionally, we removed unwanted low-frequency components by applying a high-pass filter of 1 Hz. Finally, we mathematically referenced the decimated signals to the average reference voltage to reduce biases in the analysis of the potential distribution (Bertrand et al, 1985; Murray et al, 2008). This step has no effect on the estimation of the scalp electric field, for it is a reference-free quantity by definition.

In order to enhance the signal-to-noise ratio, we averaged same-class trials over small groups of trials before performing recognition. We fixed the number of samples per average trial according to the amount of classes and total number of trials available in the experiment. With this consideration in mind, the number of samples per average trial varied as follow: 12 (Exp. I, 8 initial consonants); 5 (Exp. I, 32 syllables); 20 (Exp. I, 4 vowels); 5 (Exp. II); and 5 (Exp. III).

Approximation for the normal component of the scalp electric field

In conventional EEG no information about the electric potential is available along the direction normal to the scalp, which precludes a direct estimation of the field normal component. Our approach to circumvent this problem consists of an approximation based on the theoretical considerations explained below.

The widely-used spherical head model is assumed for simplicity throughout this paper, taking the outer scalp surface as a sphere of homogeneous isotropic conductivity σ^{scalp} and radius r_{scalp}. The orthogonal components describing the field are E_θ, E_φ, and E_r; two of them (E_θ and E_φ) are tangent to the scalp and the other (E_r) is normally-oriented. These components are obtained from the electric potential Φ by using

$$E_r = -\frac{\partial \Phi}{\partial r}, \quad E_\theta = -\frac{1}{r}\frac{\partial \Phi}{\partial \theta}, \quad E_\varphi = -\frac{1}{r\sin\theta}\frac{\partial \Phi}{\partial \varphi}. \tag{1}$$

Note that our convention of spherical coordinates is that of Griffiths (1999, p. 38). The polar angle θ increases down from the vertex and the azimuth φ from the nasion counterclockwise around the vertex.

We recall that the normal component of the electric field is subject to the condition that its product by the electrical conductivity is constant at any interface between two adjacent macroscopic layers in the head (Plonsey, 1969, ch. 5). For homogeneous layers with conductivities σ^1 and σ^2 this condition reads

$$\sigma^1 E_r^1 = \sigma^2 E_r^2, \tag{2}$$

According to this relation, any sudden change in the electrical conductivity at a tissue interface is accompanied by the reciprocal change of the field normal component. If we apply (2) to the scalp-air interface, and consider the negligibility of σ^{air} as compared to σ^{scalp} (typically $\sigma^{\mathrm{air}}/\sigma^{\mathrm{scalp}} \sim 10^{-14}$), we obtain

$$\sigma^{\mathrm{scalp}} E_r^{\mathrm{scalp}} \approx 0, \tag{3}$$

so that the field normal component is approximately zero everywhere on the outer scalp surface. Therefore, the scalp electric field is essentially a tangential field along the free scalp surface. Recalling that the scalar potential obeys Laplace's equation $\nabla^2\Phi = 0$ anywhere in the extracellular region,

$$\frac{2}{r}\frac{\partial\Phi}{\partial r} + \frac{\partial^2\Phi}{\partial r^2} + \frac{1}{r^2\sin\theta}\frac{\partial}{\partial\theta}\left(\sin\theta\,\frac{\partial\Phi}{\partial\theta}\right) + \frac{1}{r^2\sin^2\theta}\frac{\partial^2\Phi}{\partial\varphi^2} = 0, \tag{4}$$

or

$$\nabla^2_{\mathrm{surf}}\Phi = \frac{2}{r}E_r + \frac{\partial E_r}{\partial r}, \tag{5}$$

where ∇^2_{surf} is the surface Laplacian operator and $\partial E_r/\partial r$ represents the outward normal derivative of E_r. Since E_r^{scalp} is null, we obtain from (5)

$$\nabla^2_{\mathrm{surf}}\Phi\big|_{\mathrm{scalp}} = \left.\frac{\partial E_r}{\partial r}\right|_{\mathrm{scalp}}, \tag{6}$$

i.e., the surface Laplacian of Φ is equal to the rate of change of E_r along the normal direction on the scalp.

The condition (2) follows from the conservation of the *volume current density,* $\mathbf{J}^v$, that flows passively in the extracellular region due to brain activation. This density is locally related to the electric field by Ohm's law:

$$\mathbf{J}^v = \sigma\mathbf{E}. \tag{7}$$

It follows then that the vanishing of E_r^{scalp} confines the current flow within the head, i.e., $j_r^v|_{\mathrm{scalp}} = 0$, causing a significant increase in lateral spread of flow lines close to the outer scalp surface.

The application of a conductive gel or an electrolytic solution to couple a resistive electrode to the scalp changes the boundary conditions locally, affecting the behavior of the flow lines beneath electrode sites. Now the field normal component is not constrained to vanish abruptly at these sites, but instead it drives current out of the head into measuring device. This makes the tangential current spread less pronounced than along the scalp-air interface. As a consequence, the last term on the left side of Eq. (5) should reduce its importance locally. Based on this consideration, our approach to estimate E_r^{scalp} at measurement electrode sites consists of the approximation

$$\nabla^2_{\text{surf}}\Phi|_{\text{scalp}} \approx \frac{2}{r^{\text{scalp}}} E_r^{\text{scalp}}. \tag{8}$$

That is, we assume that when EEG is actually recorded in the laboratory using resistive electrodes the surface Laplacian of Φ approximates to the normal component of the scalp electric field multiplied by the factor $2/r^{\text{scalp}}$. This approximation was used throughout this work and we tested its validity in the context of brain-wave recognition. Note that in virtue of (7) the expression (8) locally relates $\nabla^2_{\text{surf}}\Phi|_{\text{scalp}}$ to the normal component of $\mathbf{J}^v$. This goes some way toward supporting the usual view that the surface Laplacian differentiation is an accurate method to associate local EEG events generated by cortical radial dipoles to the underlying physical structure. However, the expression (8) has been reached without any assumption whatsoever about brain sources.

Numerical procedure

Numerical differentiations to estimate the scalp electric field from EEG data were carried out at low computational cost using splines on the spherical head model. Consider an instantaneous scalp potential distribution $\{V_1, \cdots, V_N\}$, sampled at electrode locations $\mathbf{r}_1, \cdots, \mathbf{r}_N$ at a time t. The 3D spline interpolant is the function defined by

$$f_\lambda(\mathbf{r}) = \sum_{j=1}^{N} c_j \left\|\mathbf{r} - \mathbf{r}_j\right\|^{2m-3} + \sum_{\ell=1}^{M} d_\ell \, \phi_\ell(\mathbf{r}), \tag{9}$$

where $m > 2$ is an integer, $M = \binom{m+2}{3}$ is subject to $M < N$, $\phi_1, \cdots, \phi_M$ are a set of linearly-independent polynomials in $\mathbb{R}^3$ of degree less than m, and c_j and d_j are parameters that depend on the potential distribution. In order to avoid the magnification of high-frequency spatial noises, the parameters c_j and d_j were determined by introducing a regularization parameter, λ. This lead us to the system

$$\begin{pmatrix} \mathbf{K} + N\lambda\mathbf{I} & \mathbf{T} \\ \mathbf{T}' & 0 \end{pmatrix} \begin{pmatrix} \mathbf{c} \\ \mathbf{d} \end{pmatrix} = \begin{pmatrix} \mathbf{v} \\ \mathbf{0} \end{pmatrix}, \tag{10}$$

where $(\mathbf{K})_{ij} = \left\|\mathbf{r}_i - \mathbf{r}_j\right\|^{2m-3}$, $(\mathbf{T})_{ij} = \phi_j(\mathbf{r}_i)$, $\mathbf{c} = (c_1, \cdots, c_N)'$, $\mathbf{d} = (d_1, \cdots, d_M)'$, and $\mathbf{v} = (V_1, \cdots, V_N)'$. As explained in Carvalhaes and Suppes (2011); Carvalhaes (2012), the system (10) is singular on a spherical surface. Following Carvalhaes and Suppes

(2011), we factorize $\mathbf{T}$ as

$$\mathbf{T} = (\mathbf{Q_1}\,, \mathbf{Q_2}) \begin{pmatrix} \mathbf{R} \\ O \end{pmatrix}, \tag{11}$$

where $\mathbf{Q}_1 \in \mathbb{R}^{N\times M}$ and $\mathbf{Q}_2 \in \mathbb{R}^{N\times(N-M)}$ are orthonormal and $\mathbf{R} \in \mathbb{R}^{M\times M}$ is upper triangular, and introduce the auxiliary matrices

$$\mathbf{C}_\lambda = \mathbf{Q}_2 \left[\mathbf{Q}_2' \left(\mathbf{K} + N\lambda \mathbf{I}\right) \mathbf{Q}_2\right]^{-1} \mathbf{Q}_2', \tag{12a}$$

$$\mathbf{D}_\lambda = \mathbf{R}^{+}\mathbf{Q}_1' \left(\mathbf{1} - \mathbf{K}\mathbf{C}_\lambda - N\lambda \mathbf{C}_\lambda\right), \tag{12b}$$

where $\mathbf{R}^{+}$ is the pseudo-inverse of $\mathbf{R}$. Let $\mathbf{e}_\lambda^\theta$, $\mathbf{e}_\lambda^\varphi$, and $\mathbf{e}_\lambda^r$ be N-dimensional vectors giving the respective components of the scalp electric field at the electrode coordinates. These vectors can be obtained by linearly transforming $\mathbf{v}$ as follows:

$$\mathbf{e}_\lambda^\theta = \left(\mathbf{K}_\theta \mathbf{C}_\lambda + \mathbf{T}_\theta \mathbf{D}_\lambda\right)\mathbf{v} = \mathbf{E}_\lambda^\theta \mathbf{v}, \tag{13a}$$

$$\mathbf{e}_\lambda^\varphi = \left(\mathbf{K}_\varphi \mathbf{C}_\lambda + \mathbf{T}_\varphi \mathbf{D}_\lambda\right)\mathbf{v} = \mathbf{E}_\lambda^\varphi \mathbf{v}, \tag{13b}$$

$$\mathbf{e}_\lambda^r = \left(\tilde{\mathbf{K}} \mathbf{C}_\lambda + \tilde{\mathbf{T}} \mathbf{D}_\lambda\right)\mathbf{v} = (r^{\text{scalp}}/2)\mathbf{L}_\lambda \mathbf{v}. \tag{13c}$$

The analytic expressions for the matrices $\mathbf{K}_\theta$, $\mathbf{T}_\theta$, $\mathbf{K}_\varphi$, $\mathbf{T}_\varphi$, $\tilde{\mathbf{K}}$, and $\tilde{\mathbf{T}}$ and a Matlab code implementation are available online in the supplementary material. We remark that the vector $\mathbf{e}_\lambda^r$ was obtained as the surface Laplacian of $\mathbf{v}$ following Eq. (8). Since the field components are reference-free by definition, the linear transformations (13) are all singular, regardless of the value of λ.

Recognition procedure

For each experiment, we carried out channel-by-channel recognition using a 10-fold cross-validation on linear discriminant analysis (Parra et al, 2008; Suppes et al, 2009). We organized the data in a matrix form, with different trials occupying different rows and the time samples spanning the columns. To reduce temporal features from the data in order to optimize performance we applied Principal Component Analysis (PCA).. We repeated this procedure several times for that recognition for each data matrix, adding the principal components one by one in order of decreasing variance in the data. We performed this computation after determining the optimal value of λ, sought in the range 0.001-100 in a 50-points log-scale grid.

Our ultimate goal was to compare cross-validated rates provided by the potential distribution and electric field estimate. However, we found instructive to examine the effect of the normal and tangential components of the scalp electric field separately.

For that we carried out recognition using the field normal component alone, and for a two-vector field composed by the field tangential components. Henceforth we refer to these derivations simply as *normal field* and *tangential field*, respectively. We obtained the matrix representation of vector fields through one-by-one concatenation of trials, resulting in a matrix with twice (tangent field) or three times (total field) as many columns as the number of samples per trial.

Statistical analysis

We used the same random sequence of trials in the recognition of the four waveforms (potential, normal field, tangential field, and total field), thus giving pairwise recognition rates to compare performance. The practical effect of the electric field and its components was separately compared to the potential in terms of effect sizes with 95% confidence intervals. Effect sizes (*ES*) were calculated as

$$\mathrm{ES}_i = \frac{\mu_i - \mu_{\mathrm{pot}}}{s_{i,\mathrm{pool}}}, \tag{14}$$

where μ is the mean recognition rate over all participants, the index i stands for either normal field, tangential field, or total field, and μ_{pot} is the mean rate for the potential. The pooled standard deviation $s_{i,\mathrm{pool}}$ is defined by $s_{i,\mathrm{pool}} = \sqrt{(s_i^2 + s_{\mathrm{pot}}^2)/2}$, where s^2 is the variance and the index i is the same as above. The approximate width of the respective 95% confidence interval (95%CI) was given by

$$95\%\mathrm{CI} = [\mathrm{ES} - 1.96\, s_e\, , \mathrm{ES} + 1.96\, s_e], \tag{15}$$

where s_e is the asymptotic standard error between paired rates (Nakagawa and Cuthill, 2007).

Results

Recognition rates

Tables 1-5 summarize the results we found for the recognition rates of each experiment. The highest cross-validation mean rate is shown for each participant along with the best sensor. In general, the rates were remarkably good bearing in mind the chance level of each experiment. The total electric field was the best predictor, except for Exp. III, where it performed similarly to the tangential field.

Table 1 shows the result for the 8-class problem in which the initial consonants of Exp. I were used as labels. The total electric field not only yielded the highest recognition rate for all participants, but interestingly its best performance was always achieved on locations at the primary auditory cortex (A1). Averaged over all participants, the total field improved 10.6% over the potential and outperformed the field normal component in 4.8%. The tangential field performed similarly to the total field in average, but the individual rates of the total field were higher than those of the tangential field for all participants.

Table 1: Highest performance for the recognition of the 8 initial consonants of Exp. I.

	potential		norm. field		tang. field ‘		total field	
participant	%	sensor	%	sensor	%	sensor	%	sensor
S1	45.2	E36	57.5	E41	60.7	E40	63.0	E40,E41
S2	37.2	E30	40.5	E12	43.4	E109	44.4	E40
S3	27.5	E13,E29	32.6	E28	36.0	E47	38.8	E35
S4	31.9	E112	30.3	E20	31.9	E122	32.4	E41
Avg.±std.	35.9±7.4		41.7±11.9		44.6±12.1		46.5±12.5	

Trials per participant: S1 - 600, S2 - 304, S3 - 528, and S4 - 376. Chance level: 12.5%.

Table 2 gives the result for the recognition of the 32 syllables of Exp. I. The 4-fold increase in the number of classes as compared to the recognition of the initial consonants resulted in a decrease in recognition rate by almost the same factor. The total field once again provided the highest recognition rates, except for S4, for which it yielded the rate 8.1% vs. 8.2% by the tangential field. We see that the highest rates of both methods were achieved in the region of the secondary auditory cortex (A2).

Table 2: Highest performance for the recognition of the 32 syllables of Exp. I.

	potential		norm. field		tang. field ‘		total field	
participant	%	sensor	%	sensor	%	sensor	%	sensor
S1	13.4	E36	21.4	E41	19.6	E46	23.1	E41
S2	9.5	E30	9.9	Cz	10.9	E35	11.0	E40
S3	7.8	E13	8.4	E20	9.3	E97	9.4	E44,E46
S4	7.9	E6,E13	7.1	E12	8.2	E116,E122	8.1	E116,E122
Avg.±std.	10.0±2.5		12.7±6.3		12.8±5.0		14.0±6.7	

Trials per participant: S1 - 1440, S2 - 736, S3 - 1280, and S4 - 897. Chance level: 3.1%.

Table 3 summarizes the result of the recognition of the 4 vowels in Exp. I. Despite the rates being significantly above chance probability (25%), the highest rate of 46.9% (S1) is much lower than that of the initial consonants (63%, S1), which had twice as many classes. Furthermore, average improvements were not as large in average as the two previous cases.

Table 3: Highest performance for the recognition of the 4 vowels of Exp. I.

	potential		norm. field		tang. field		‘	total field	
participant	%	sensor	%	sensor	%	sensor		%	sensor
S1	40.8	E37	46.4	E42	41.1	E40		46.9	E41
S2	38.3	E52	38.3	E80	43.9	E56		43.3	E56
S3	37.0	E6	39.6	E127	38.3	E52		38.6	E111
S4	39.6	E76	39.6	E76	44.4	E97		41.8	E105
Avg.±std.	39.0±1.6		41.6±3.5		41.4±2.5			42.8±3.4	

Trials per participant: S1 - 360, S2 - 180, S3 - 316, S4 - 225. Chance level: 25.0%.

Table 4 shows the recognition rates of Exp. II. The lowest recognition rate was 52.1% for S2 using the normal component of the scalp electric field alone. The highest rate 86.9% was achieved with participant S1 using the total field. These results are remarkably good taking into account the chance probability of 11.1%. Recognition using only the tangential components or the total field significantly outperformed the potential and normal field. The normal field performed similarly to the potential in average (63.0% vs. 61.9%) and rendered the highest standard deviation among all methods.

Table 4: Highest performance for the recognition of the 9 images of Exp. II.

	potential		norm. field		tang. field		‘	total field	
participant	%	sensor	%	sensor	%	sensor		%	sensor
S1	72.7	PO8	81.6	PO8	83.2	PO4		86.9	PO8
S2[a]	58.2	O9	52.1	O2	68.0	PO4		71.1	O2
S3	61.7	POz	60.6	P3	62.2	CP2		70.7	P3,P4
S4[b]	59.5	POz	63.9	PO8	68.1	O2		75.1	PO8
S5	66.1	PO3	70.5	POz	76.2	P1		81.8	POz
S6[a]	60.3	O1	55.9	O2	65.8	CP4		70.0	Oz
S7[a]	54.8	Iz	56.6	P2	67.5	P4		70.6	P4
Avg.±std.	61.9±5.9		63.0±10.2		70.2±7.1			75.2±6.7	

[a]Channels CP6 and PO9 were off. [b]Channel CP6 was off.

Trials per participant: 543 . Chance level: 11.1%.

Table 5 shows the recognition rates for the trials of the mental task of Exp. III. Observe that these rates are higher than those showed in Carvalhaes and Suppes (2011). The reason for this difference is because in Carvalhaes and Suppes (2011) the recognition was performed without averaging the trials to reduce temporal noise. Here, most of the best predictions were achieved by the tangential electric field (S2, S3, S4, S7, S9, S10, S11) rather than the total field itself, which yielded the highest rate for only 5 participants (S3, S6, S8, S9, S11). The normal field was the most accurate method for participants S1 and S5.

Table 5: Highest performance for the recognition of the mental task of Exp. III.

	potential		norm. field		tang. field		total field	
participant	%	sensor	%	sensor	%	sensor	%	sensor
S1	95.9	P8	96.7	P8	95.0	CP6	95.9	P8
S2	77.7	FC4	78.5	C4	83.5	P3	81.8	P1
S3	81.0	PO4	81.0	CPz	86.0	P2	86.0	CP4
S4	86.7	P7	82.5	Pz	89.2	P1,P2	88.3	P4,PO4
S5	86.0	P4	92.6	P4	88.4	CPz	88.4	P4
S6	68.3	P7,P3,PO3	72.5	F7,FC3	73.3	FT7	74.2	Pz
S7	79.3	PO3,O1	86.8	PO3	87.6	O1	85.1	P3
S8	87.6	O1	81.0	C3,C6,O2	90.9	P3	91.7	PO3
S9	77.7	C4	76.0	TP9,PO3	80.2	PO4	80.2	PO4
S10	88.4	FC2,FC4	86.8	P3	93.4	CP3	92.6	CP3
S11	82.6	FC2	86.0	P7	86.8	CP3	86.8	CP5,CP3,P3
Avg.±std.	82.8±7.3		83.7±7.1		86.7±6.1		86.4±6.1	

Trials per participant: 121. Chance level: 50%.

Effect sizes

We evaluated the practical significance of improvements in the recognition rates shown above in terms of effect sizes and 95% confidence intervals. The result is summarized in Table 6. The tasks of recognizing the 8 initial consonants and 32 syllables in Exp. I rendered nearly the same effect size. The recognition of the 4 vowels, where the deviation from the mean recognition rate was relatively small for each participant, resulted in effect sizes equal to or greater than one standard deviation. The effect sizes were all positive in Exp. II, but the confidence interval for the normal field included zero. This means that the hypothesis of no difference in performance between the potential and normal field cannot be rejected at 95% level of confidence in this case. In contrast, the superior performance of the total electric field as compared to the potential was confirmed with 2.1 standard deviations. The effect sizes were all positive in Exp. IV, but again the hypothesis of no difference between the potential and the normal field cannot be rejected since the confidence interval includes zero.

Table 6: Effect sizes and 95% confidence intervals for improvements in recognition rates.

Experiment	normal field	tangential field	total field
Exp. I (initial consonants)	0.6 (0.4 to 0.8)	0.9 (0.6 to 1.2)	1.0 (0.7 to 1.4)
Exp. I (syllables)	0.6 (0.4 to 0.7)	0.7 (0.5 to 0.9)	0.8 (0.6 to1.0)
Exp. I (vowels)	1.0 (0.6 to 1.3)	1.2 (0.6 to 1.7)	1.4 (1.0 to 1.9)
Exp. II	0.1 (-0.2 to 0.3)	1.3 (0.4 to 2.1)	2.1 (0.9 to 3.4)
Exp. III	0.1 (-0.2 to 0.5)	0.6 (0.3 to 0.9)	0.5 (0.3 to 0.8)

Effect of smoothing

Additionally, we evaluated the possible effect of smoothing the data in the recognition rates. For that, the potential distribution was spatially smoothed using the same procedure described for the scalp electric field. So, recognition was repeated 50 times for each participant, with the smoothing parameter λ varying in the same interval that optimized the performance of the electric field. However, we found no significant change in the rates by using this procedure. The largest effect size for the smoothed potential compared with raw data was 0.3 (95%CI, 0.2–0.5). This result occurred for the recognition of the 8 initial consonants (Exp. I). The other experiments rendered effect sizes smaller than 0.3, and the confidence interval included zero in all cases.

Recognition with multiple channels

We also evaluated the applicability of the electric field in multichannel recognition. For that, the best performing channels were concatenated in groups of 5 and 10 channels independently of their physical location, and the trials were then recognized using the same optimization procedure described above for single channels. Table 7 shows the resulting effect sizes. (The tables showing the recognition rates are presented in the supplementary material available online.).

Small variations were observed in the performance of the normal field, the most favorable one being the monotonic increase of effect size (0.6, 0.7, 0.8) in the recognition of the 8 initial consonants. The effect of the normal field in the recognition of the 4 vowels changed drastically, decreasing 10 folds with using 10 channels instead of single channels. The practical effects of the tangential field and total field were strongly affected in the recognition of the vowels, shape-color images, and stop-go imaginations. They remained about the same in the two other cases, excepted that the effect of the electric field decreased from 1.0 to 0.5 in the recognition of the initial consonants using 10 channels. Differently from single-channel recognition, the 95%

confidence interval includes zero in several cases, indicating total loss of significance of improvements in recognition rate.

Table 7: Effect sizes for concatenating the 5 and 10 best-performing channels. The columns account for the normal component (NC), the tangential components (TC), and the total scalp electric field (TF).

	Five channels			Ten channels		
Experiment	NC	TC	TF	NC	TC	TF
Exp. I (initial consonants)	0.7	0.8	0.8	0.8	0.8	0.5
Exp. I (syllables)	0.7	0.6	0.8	0.6	0.8	0.6
Exp. I (vowels)	0.4	0.1	−0.1*	0.1*	-0.4*	−0.9
Exp. II	−0.2*	0.1	0.4	0.2*	0.2*	0.3*
Exp. III	0.0*	−0.2*	−0.4*	0.1*	0.0*	−0.3*

*95%CI includes zero.

Discussion

This work demonstrated the effectiveness of the scalp electric field in the recognition of brain processes represented in EEG signals. In general, the recognition accuracy of our experiments was higher using all components of the electric field instead of normal or tangential components separately. The mental task of Exp. III was the only case for which the average recognition rate of the tangential field was higher than that of the total electric field.

Improvements were generally much less significant in the case of multichannel recognition. In general, the potential substantially improved performance with multiple channels, but the performance of the electric field increased only slightly, thus reducing the effect size in more than one standard deviation in some cases. The recognition of the visual-evoked responses of Exp. II was the case for which this reduction was more significant.

Recognizing vowels from syllables was the most challenging task encountered in our study. The comparatively low rates achieved in this case were possibly related to variations in the onset of vowels preceded by different consonants. As long-duration consonants take longer to be perceived as compared to short consonants, the onset of the ensuing vowel varied affecting the recognition negatively. Evidence of variations in onset was reported, for instance, by Lawson and Gaillard (1981) based on the analysis of evoked potential.

Although the approximation (8) for the field normal component was obtained assuming the spherical head model, there appears no major difficulty in extending this result to more realistic geometries at first sight, e.g., the slightly more realistic ellipsoidal scalp model. Also, experimental results pointed out that the electrical conductivity of the scalp has a prominent directional dependency that requires a representation of the scalp conductivity as a 2nd-rank symmetric tensor (Abascal et al, 2008; Petrov, 2012). Specially important is the tangential:radial anisotropy ratio of about 1.5, which would be accounted for by writing

$$\boldsymbol{\sigma}^{\text{scalp}} = \sigma_r^{\text{scalp}}\hat{\mathbf{r}}\hat{\mathbf{r}} + \sigma_t^{\text{scalp}}\hat{\boldsymbol{\theta}}\hat{\boldsymbol{\theta}} + \sigma_t^{\text{scalp}}\hat{\boldsymbol{\varphi}}\hat{\boldsymbol{\varphi}}, \tag{16}$$

where σ_r^{scalp} and σ_t^{scalp} are real-valued conductivities along radial and tangential directions. However, the only change in (8) due to (16) is the multiplication of $\nabla^2_{\text{surf}}\Phi$ by the ratio $\sigma_t^{\text{scalp}}/\sigma_r^{\text{scalp}} \approx 1.5$, which has no practical effect on the recognition rates.

Acknowledgements

We would like to thank Dr. Gary Oas and Prof. José Paulo de Mendonça for fruitful discussions on the electric field of the brain. We are also in debt with Dr. Rui Wang for her help in all matters related to Exp. I.

References

Abascal JFPJ, Arridge SR, Atkinson D, Horesh R, Fabrizi L, Lucia MD, Horesh L, Bayford RH, Holder DS (2008) Use of anisotropic modelling in electrical impedance tomography: description of method and preliminary assessment of utility in imaging brain function in the adult human head. Neuroimage 43:258–268

Babiloni C, Carducci F, Cincotti F, Rossini PM, Neuper C, Pfurtscheller G, Babiloni F (1999) Human movement-related potentials vs desynchronization of EEG alpha rhythm: a high-resolution EEG study. Neuroimage 10:658–665

Babiloni C, Babiloni F, Carducci F, Cincotti F, Percio CD, Pino GD, Maestrini S, Priori A, Tisei P, Zanetti O, Rossini PM (2000) Movement-related electroencephalographic reactivity in Alzheimer disease. Neuroimage 12:139–146

Babiloni C, Babiloni F, Carducci F, Cincotti F, Cocozza G, Percio CD, Moretti DV, Rossini PM (2002) Human cortical electroencephalography (EEG) rhythms during the observation of simple aimless movements: a high-resolution EEG study. Neuroimage 17:559–572

Babiloni F, Cincotti F, Bianchi L, Pirri G, del R Millán J, Mourino J, Salinari S, Marciani MG (2001) Recognition of imagined hand movements with low resolution surface Laplacian and linear classifiers. Med Eng Phys 23:323–328

Bai O, Lin P, Vorbach S, Floeter MK, Hattori N, Hallett M (2008) A high performance sensorimotor beta rhythm-based brain-computer interface associated with human natural motor behavior. J Neural Eng 5:24–35

Bertrand O, Perrin F, Pernier J (1985) A theoretical justification of the average reference in topographic evoked potential studies. Electroencephalogr Clin Neurophysiol 62:462–464

Besio WG, Kay SM, Liu X (2009) An optimal spatial filtering electrode for brain computer interface. Conf Proc IEEE Eng Med Biol Soc 2009:3138–3141

Carvalhaes CG (2012) Spline interpolation on nonunisolvent sets. IMA Journal of Numerical Analysis (in press)

Carvalhaes CG, Suppes P (2011) A spline framework for estimating the EEG surface Laplacian using the Euclidean metric. Neural Comput 23:2974–3000

Carvalhaes CG, Perreau-Guimaraes M, Grosenick L, Suppes P (2009) EEG classification by ICA source selection of Laplacian-filtered data. In: Proc. IEEE Int. Symp. Biomedical Imaging: From Nano to Macro ISBI '09, pp 1003–1006

Chen GS, Lu CC, Chen CW, Ju MS, Lin CC (2005) Portable active surface laplacian eeg sensor for real-time mu rhythms detection. Conf Proc IEEE Eng Med Biol Soc 5:5424–5426

Griffiths DJ (1999) Introduction to Electrodynamics, 3rd ed. Prentice Hall, New Jersey

Hjorth B (1975) An on-line transformation of EEG scalp potentials into orthogonal source derivations. Electroencephalogr Clin Neurophysiol 39:526–530

Kayser J, Tenke CE (2006a) Principal components analysis of Laplacian waveforms as a generic method for identifying ERP generator patterns: I. Evaluation with auditory oddball tasks. Clin Neurophysiol 117:348–368

Kayser J, Tenke CE (2006b) Principal components analysis of Laplacian waveforms as a generic method for identifying ERP generator patterns: II. Adequacy of low-density estimates. Clin Neurophysiol 117:369–380

Lawson EA, Gaillard AW (1981) Evoked potentials to consonant-vowel syllables. Acta Psychol (Amst) 49:17–25

Murray MM, Brunet D, Michel CM (2008) Topographic ERP analyses: a step-by-step tutorial review. Brain Topogr 20:249–264

Nakagawa S, Cuthill IC (2007) Effect size, confidence interval and statistical significance: a practical guide for biologists. Biol Rev Camb Philos Soc 82:591–605

Nunez PL, Pilgreen KL (1991) The spline-Laplacian in clinical neurophysiology: a method to improve EEG spatial resolution. J Clin Neurophysiol 8:397–413

Nunez PL, Srinivasan R (2006) Electric Fields of the Brain: The Neurophysics of EEG, 2nd edn. Oxford University Press, New York

Nunez PL, Westdorp AF (1994) The surface Laplacian, high resolution EEG and controversies. Brain Topogr 6:221–226

Nunez PL, Pilgreen KL, Westdorp AF, Law SK, Nelson AV (1991) A visual study of surface potentials and Laplacians due to distributed neocortical sources: computer simulations and evoked potentials. Brain Topogr 4:151–168

Nunez PL, Silberstein RB, Cadusch PJ, Wijesinghe RS, Westdorp AF, Srinivasan R (1994) A theoretical and experimental study of high resolution EEG based on surface Laplacians and cortical imaging. Electroencephalogr Clin Neurophysiol 90:40–57

Oostenveld R, Praamstra P (2001) The five percent electrode system for high-resolution EEG and ERP measurements. Clinical Neurophysiology 112:713–719

Parra LC, Christoforou C, Gerson AD, Dyrholm M, Luo A, Wagner M, Philiastides MG, Sajda P (2008) Spatiotemporal linear decoding of brain state. Signal Proc Mag, IEEE 25:107–115

Perrin F, Pernier J, Bertrand O, Echallier JF (1989) Spherical splines for scalp potential and current density mapping. Electroencephalogr Clin Neurophysiol 72:184–187

Petrov Y (2012) Anisotropic spherical head model and its application to imaging electric activity of the brain. Phys Rev E 86:011,917

Plonsey R (1969) Bioelectric Phenomena. McGraw-Hill, New York

Srinivasan R, Nunez PL, Tucker DM, Silberstein RB, Cadusch PJ (1996) Spatial sampling and filtering of EEG with spline Laplacians to estimate cortical potentials. Brain Topogr 8:355–366

Suppes P, Perreau-Guimaraes M, Wong DK (2009) Partial orders of similarity differences invariant between EEG-recorded brain and perceptual representations of language. Neural Comput 21:3228–3269

Wang R (2011) Recognizing phonemes and their distinctive features in the brain. PhD thesis, Stanford University

Wang R, Perreau-Guimaraes M, Carvalhaes C, Suppes P (2012) Using phase to recognize English phonemes and their distinctive features in the brain. Proc Nac Acad Sci (in press)